MEASUREMENTS OF THE THERMAL CHARACTERISTICS OF COPPER - WATER HEAT PIPE AT VARIOUS ORIENTATIONS

Mohamed A. Aziz.
Department of Mechanical Power Engineering, Faculty of Engineering,
Zagazig University, Zagazig, Egypt.

ABSTRACT

An experimental study of the thermal characteristics of water copper heat pipe at various orientations has been conducted. Investigations included the analysis of the experimental data showed that, the heat pipe sonic, entrainment, and boiling limits are approximately competent irrespective of the heat pipe orientation. The heat transfer capillary limitation was shown to be the most dominating factor which is mainly affected by the heat pipe orientation, wick wetness, and bubble nucleation. The mechanism describing the capillary limit behaviour is reported. The heat pipe in the horizontal orientation exhibiting low vapor-wall temperature difference, having high value of the heat transfer coefficient is seemed to be the most acceptable from the point of view of heat transfer .

Keywords: Heat Pipe. Screen Matrix.

NOMENCLATURE

A	area (m^2)
C_s	wetted perimeter of wick surface pore (m)
D	diameter, (m)
F	friction coefficient (Pa/W.m)
$(f_v.R_{ev})$	drag coefficient = 16 defined in [18]
f	force (N)
K	wick permeability (m^2)
K_1, K_2	constant of proportionality in Weber number
k	conductivity (W/mK)
L	length (m)
M,	Mach number eq.(8)
m	mass flow rate, (kg/s)
N	screen mesh number (m^{-1})
P	pressure, (Pa)
Q	heat transfer limit (W)
R	thermal resistance (m^2 K/W)
Re	Reynolds number eq. (7)
r	radius (m)
S	crimping factor = 1.05 defined in [18]
T	temperature, (K)
t	thickness, (m)
U	overall heat transfer coefficient (W/m^2K)
V	velocity, (m/s)
W	width, (m)
We	Weber number $[(K_1.\ \rho_v V_v^2.A_s)/(2K_2.C_s\sigma)]$

Greek Symbols

ρ	density (kg/m^3)
ν	viscosity (kg/ms)
σ	surface tension, (N/m)
λ	latent heat, (J/kg)
ϵ	wick porosity
γ	specific heat ratio
φ	inclination angle, (rad)
Δ	difference

Subscripts

a	adiabatic
b	boiling
c	condenser, capillary
cm	maximum capillary
e	evaporator, entrainment
eff	effective

hs surface pore hydraulic
hv vapor hydraulic
i inner
l liquid
max maximum
n critical nucleation
o outer
p pipe
pm maximum effective pumping
s sonic surface pore, shear force, of wick
v vapor, vapor core
t total
w wick, wick wire
x axial

INTRODUCTION

The heat pipe is a device for transmitting heat from one location to another with small temperature gradient. It has found great interest in terrestrial applications, such as heat recovery, energy conservation, solar energy utilization, soil warming and space technology. Understanding the thermal characteristics of the heat pipes is of interest to many space and terrestrial applications. Numerous theoretical and experimental studies of the thermal characteristics of both the low and high temperatures heat pipes have been reported. Frolov et.al. [1] proposed a technique allowing calculation of the axial load and other characteristics of a heat pipe serving as an intermediate coolant. An experimental and analytical investigation has been performed by Peterson and Babin [2-4] to clarify the phenomena that govern the performance limitations and operating characteristics of micro-heat pipes. Performance analysis of the heat pipe heat exchangers based on conductance model was developed by Huang and Tsuei [5]. In this analysis, the specific heat conductance of the heat pipe was obtained from a performance test of single heat pipe. An analytical model of vapor flow in high temperature heat pipe was suggested by Flaro Dobran [6]. In his model it has been shown that, the axial heat transfer capacity (limited by the sonic heat transfer limit) depends on the working fluid, vapor flow area, the manner of the liquid evaporation into the vapor core and the heat pipe geometry. Analysis of flow and the heat transfer characteristics of an asymmetrical flat plate heat pipe has been done by Vafai and Wang [7] . In this study, the axial pressure and temperature distributions for both liquid and vapor phases were obtained. Yamamoto and Tanaka [8] investigated the heat transfer rate for sodium-steel heat pipes having three kinds of screen layers. Their results, which were obtained in the temperature range from 500 to 700 °C agreed with the proposed model based on the effective thermal conductivity. An analytical model predicting the peak-dryout steady state heat transfer limits in sintered-wick structure heat pipes was proposed by Pruzan et.al. [9]. Using this model, the flat plate and cylindrical wick heat pipe performance was evaluated. In the last decade, the most intensive contribution in heat pipe investigations are those due to Faghri et.al. [10-14]. Their works cover both analytical and experimental methods. The aim of their works was to develop numerical and experimental verification of the effects of heat load distribution on the vapor temperature, wall temperature, and the heat transport capacity of heat pipes for single and multiple heat sources. Concerning low temperature heat pipe, Abo El Naser [15], experimentally predicted the wick capillary and entrainment limits for water and acetone copper heat pipes. In the same way, Crowe et.al. [16], studied the effect of the working fluids (water and R11) properties on the entrainment and capillary limits of porous horizontal heat pipe. The transient response of horizontal water heat pipe has been studied by EL Genk and Huang [17]. In this study the effect of the input power and the cooling rate was reported.

Although the results of several experiments of water heat pipe have been published, the measurements of the thermal characteristics are believed to be inconclusive. Therefore, additional experimental measurements are needed for a rather clearer understanding of the thermal characteristics of water heat pipes.

In this work; experimental testing included the measurements of temperatures of wall and vapor distribution, along the entire length of screen matrix wicked heat pipe in various inclination angle orientations. The heat transfer boiling sonic, entrainment and capillary limits specifying the operational characteristics were predicted and justificated according to the proposed boiling

mechanism. Finally the heat transfer coefficient based upon the most effective thermal resistances was found.

ANALYSIS

The heat pipe heat transfer limits

The basic configuration of a heat pipe used in the heat transfer analysis is illustrated in Figure (1). It consists of a container such as a pipe whose interior wall is lined with a porous wick structure, saturated with working fluid. When heat is applied to the evaporator, the liquid is evaporated and the resulting vapor flows into the condenser zone, where the vapor condenses and releases the latent heat of vaporization. The liquid then returns to the evaporator zone through the wick due to the capillary forces acting in the wick and creating a surface tension pressure difference required to overcome the vapor and liquid pressure drops including that due to the gravitation or other externally imposed body forces. Few basic assumptions are charted here to calculate the capillary limit. These are:

- The heat pipe is properly charged by an adequate amount of working fluid.
- The cross-sectional area is relatively constant.
- The vapor and liquid temperatures are equal.
- The vapor flow regime is both laminar and incompressible. Thus according to Chi [18], Dunn and Reay [19] and Ivanovski [20] The maximum effective pumping pressure is.

$$P_{pm} = P_{cm} - \Delta P_l - \Delta P_x, \text{ (Pa)} \qquad (1)$$

where, P_{cm} = maximum capillary pressure = $2\sigma/r_c$, ΔP_l = normal hydrostatic pressure, = $\rho_l\, gd_v \cos\varphi$, and ΔP_x = axial hydrostatic pressure = $\rho_l \cdot gL_t \sin\varphi$.

The capillary heat transfer factor $(QL)_{c,max}$ is given by:

$$(QL)_{c,max} = P_{pm} / (F_l + F_v), \text{ (W.m)} \qquad (2)$$

The liquid and vapor friction coefficients F_l and F_v can be determined as outlined by Chi [18] as follows:

$$F_l = \mu_l / KA_w \rho_l \lambda, \quad \text{(Pa/W.m)} \qquad (3)$$

$$F_v = (f_v.R_{ev})\, \mu_v / 2A_v r^2_{hv} \cdot \rho_v \lambda, \text{ (Pa/W.m)} \qquad (4)$$

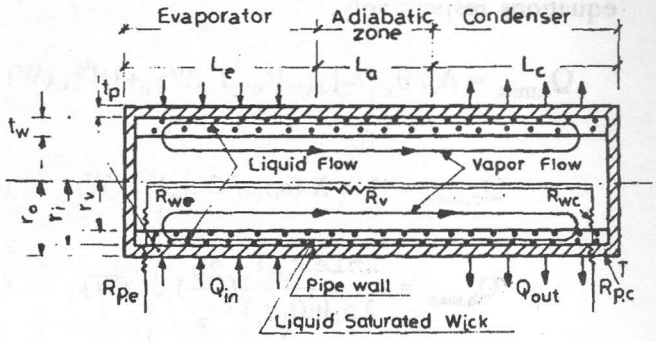

Figure 1. Sketch of heat flow path through a heat pipe.

Finally the capillary heat transfer limit $Q_{c,max}$

$$Q_{c,max} = (QL)_{c,max}/L_{eff}, \text{ (W)} \qquad (5)$$

Where L_{eff} is the heat pipe effective length, which is given by:

$$L_{eff} = [(L_c + L_e)/2] + L_a \ldots, \text{ (m)} \qquad (6)$$

Once the capillary limit has been determined these values should be checked on satisfying the conditions of laminar and incompressible flow in such a way that the Reynolds and Mach numbers of the vapor flow should satisfy the following conditions:

$$Re_v = \frac{2r_{hv} \cdot Q_{c,max}}{A_v.\mu_v.\lambda}, < 2300 \qquad (7)$$

$$M_v = \frac{Q_{c\ max}}{A_v.\rho_v.\lambda\sqrt{R_v.T_v.\gamma_v}} < 0.2 \qquad (8)$$

The depletion of liquid on the evaporator surface produces the boiling heat transfer limit. At high axial heat fluxes, the counter current flow of liquid and vapor produces the entrainment limit, where any further increase in vapor flow cannot be sustained any more increase in liquid condensate flow. When the design of a heat pipe exceeds the liquid flow limitations, the vapor flow can produce sonic and

viscous flow limitation.

Values of the sonic, entrainment and boiling limits were evaluated according to [18] by the following equations respectively:

$$Q_{s,max} = A_v \cdot \rho_v \cdot \lambda \, [\gamma_v \cdot R_v \cdot T_v/2(\gamma_v+1)]^{1/2}, \text{ (W)} \quad (9)$$

$$Q_{e,max} = A_v \cdot \lambda \, (\sigma\rho_v / 2\, r_{hs})^{1/2}, \text{ (W)} \quad (10)$$

$$Q_{b,max} = \frac{2\pi Le.k_{eff}T_v}{\lambda\rho_v \ln(r_i/r_v)}\left(\frac{2\sigma}{r_n}\right), \text{ (W)} \quad (11)$$

The remaining characteristics such as the permeability K, wick cross-sectional area, A_w vapor core cross-sectional area A_v, vapor core hydraulic radius r_{hv}, surface pore hydraulic radius r_{hs}, critical nucleation radius r_n, and the effective thermal conductivity for the liquid saturated wick k_{eff} can be determined as outlined by Chi [18].

The Heat Transfer Coefficient

The heat transfer coefficient of the heat pipe is of interest in determining its suitability for a particular application. The coefficient of heat transfer based on cross-sectional area can be found by evaluating the overall thermal resistance of the heat pipe, as follows:

$$Q = A_p U_{HP}(T_{p,e} - T_{p,c}) = \frac{A_p.(T_{pe} - T_{pc})}{\sum R}, \text{ (W)} \quad (12)$$

Where the overall coefficient of heat Transfer U_{Hp} is equal to $1/\Sigma R$. The most dominating thermal resistances based upon the overall cross-sectional area of the heat pipe are, the pipe wall at the evaporator and condenser R_{pe} and $R_{p,c}$, the saturated wick at the evaporator and condenser $R_{w,e}$ and $R_{w,c}$ and the vapor flow from the evaporator to the condenser R_v. It is worthnoting that, for the heat pipe investigated here, the values of resistance of the vapor R_v is too small compared to the other four resistances R_{pe}, R_{pc}, R_{we} and R_{wc} so that it can be neglected. The resistances R_{pe}, R_{pc}, R_{we} and R_{wc} can be determined as follows [18]:

$$R_{p,e} = \frac{r_o t_p}{2L_e \cdot k_p}, \text{ (m}^2\text{K/W)} \quad (13)$$

$$R_{p,c} = \frac{r_o t_p}{2L_c \cdot k_p}, \text{ (m}^2\text{K/W)} \quad (14)$$

$$R_{w,e} = \frac{r_o^2 \cdot t_w}{2L_e \cdot r_i \cdot k_{eff}}, \text{ (m}^2\text{K/W)} \quad (15)$$

$$R_{w,c} = \frac{r_o^2 \cdot t_w}{2L_c \cdot r_i \cdot k_{eff}}, \text{ (m}^2\text{K/W)} \quad (16)$$

Once the total resistance has been calculated, the overall heat transfer coefficient can be found from equation (12).

EXPERIMENTS

Test Facility

The experiments were conducted in the Heat Transfer Laboratory of Mechanical Power Engineering Department at Zagazig University.

The main elements of the experimental test facility are shown in Figure (2) while the schematic diagram of the test rig is given in Figure (2-a), which consisted of five subsystems : the test pipe, a heat source, heat sink, measuring instrumentation, vacuum and charging system. The water heat pipe used in the experiments consists of a copper tube (20 mm ID,26 mm OD, and 650 mm long). The pipe employs six layers of 50 μm mesh diameter copper screen matrix wick which was rolled on 13 mm rod and inserted inside the tube. This construction exerts a positive tension against the heat pipe wall. The screen wire diameter and the screen wick thickness are 6.10^{-5} and $7.2.10^{-4}$m, respectively. The heat pipe container Figure (3) consists of three sections: evaporator, adiabatic and condenser sections, whose lengths are 250, 150, and 250 mm, respectively.

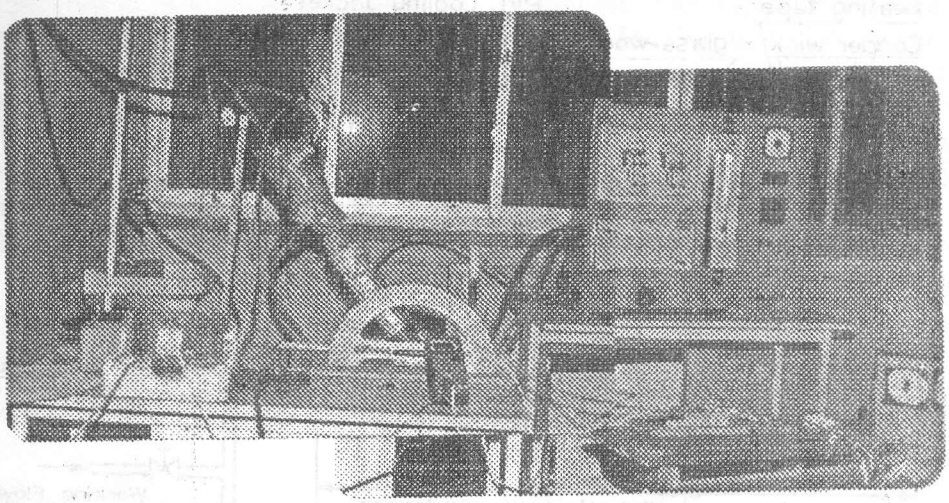

Figure 2. Photograph showing the main elements of the experimental test facility.

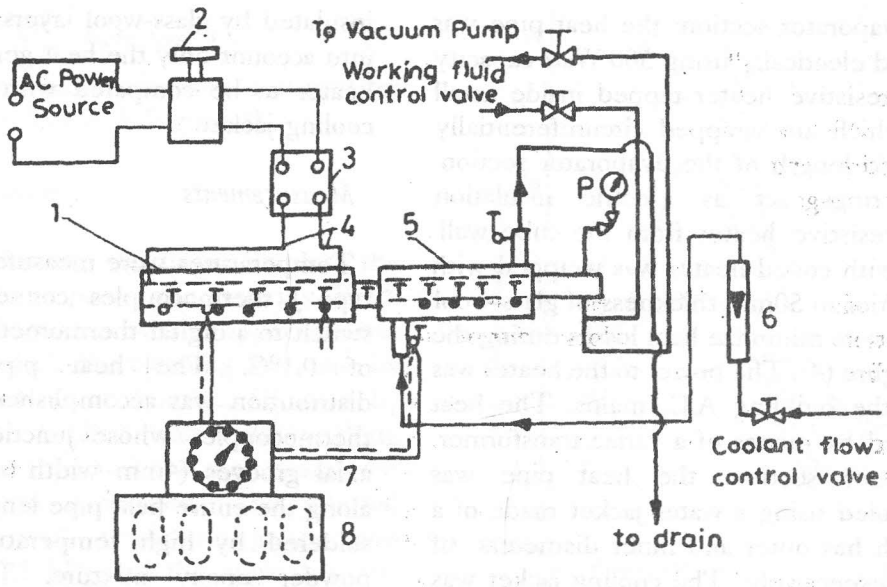

1- Heat pipe
2- Variac
3- Power meter
4- Heater leads
5- Cooling jacket
6- Coolant rotameter
7- Switching box
8- Digital thermometer
T- Thermocouple
P- Pressure gauge

Figure 2-a. Schematic diagram of the experimental set-up.

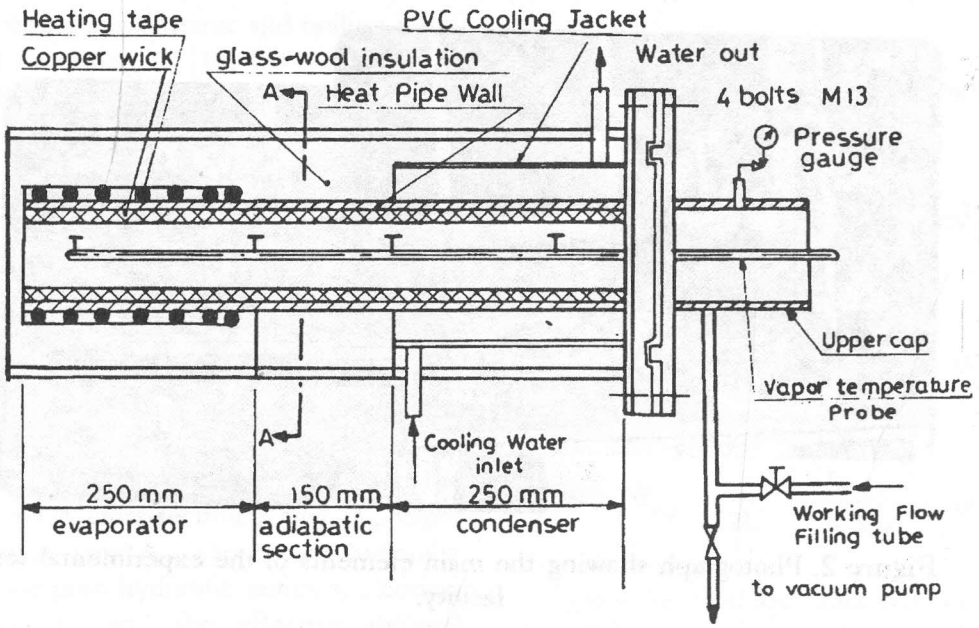

Figure 3. Details of the tested heat pipe.

Around the evaporator section, the heat pipe was uniformly heated electically using 500 Watt capacity nickel-chromic resistive heater tapped inside small ceramic rings which are wrapped circumferentially around the entire length of the evaporator section. The ceramic rings act as electric insulation separating the resistive heater from the tube wall. The heat pipe with coiled heater was wrapped with aluminum foil prior to 50mm thickness of glass-wool thermal insulation to minimize heat losses during the experiments Figure (4). The power to the heater was supplied from the building A.C. mains. The heat flux was changed by means of a variac transformer. In the condenser section, the heat pipe was convectively cooled using a water jacket made of a PVC tube which has outer and inner diameters of 60 and 54mm, respectively. The cooling jacket was connected to the building water mains via a water regulating valve by means of which the water flow rate was adjusted. The cooling jacket was covered by 50 mm layer of glass-wool insulation. At the junction section (adiabatic section) between the heated and cooled sections, a 50 mm layer of glass-wool insulation was added to provide an adiabatic surface and thus minimize any non-adiabatic effects near the junction. The entire heat pipe length was then covered by an aluminum foil sheet. It is worthnoting that, the evaporator and condenser ends were also insulated by glass-wool layers, thus ensuring to take into account only the heat generated by the electric heater to be compared with that removed at the cooling jacket.

Measurements

Temperatures were measured using iron-constant, type J thermocouples connected via change-over switch to a digital thermometer with an uncertainty of 0.1°C. The heat pipe wall temperature distribution was accomplished by means of eleven thermocouples whose junctions were laid in two axial grooves (4mm width and 2mm depth) cut along the entire heat pipe length. The grooves were soldered by high temperature resistive copper powder epoxy mixture. The location of the thermocouples junctions which were at intervals of 6 cm provided a good indication for the axial distribution of the heat pipe wall temperature. The vapor temperature inside the heat pipe was measured at four locations using specially designed probe inserted through the upper end cap of the heat pipe. Two thermocuples were used to measure the cooling water temperatures at the cooling jacket inlet and outlet. The cooling water mass flow rate was measured by means of a variable area rotameter with an accuracy of 2% of the received reading. The

input power to the heater was measured using a digital wattmeter having an accuracy of approximately of 1% of the indicated reading . The pressure of the water vapor was determined from the steam tables corresponding to the measured saturation temperature of the water in the evaporator. It was also measured by a Bourdon tube pressure gauge for confirmation.

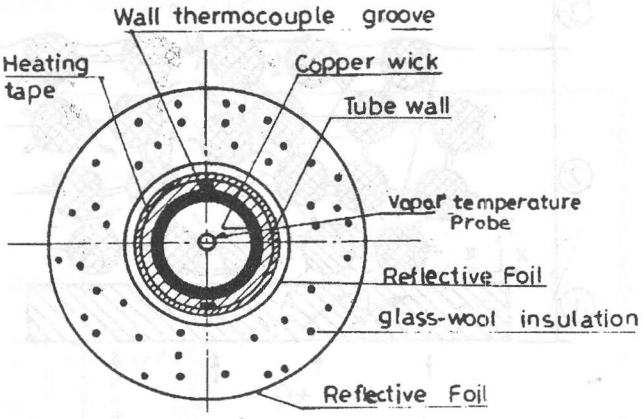

Figure 4. Transverse cross-section in the evaporator zone of the heat pipe [sec.A-A Figure 3].

Experimental Procedure.

Prior to the installation, all thermocouples, the heater and the heat pipe parts were carefully fitted. Before beginning the test runs, the apparatus was first cleaned and charged. The cleaning was made by bathing the pipe surfaces in benzne, followed by alcohol, followed by distilled water, the working fluid. Assembly of the apparatus was then completed and a vacuum pump connected. The internal pressure, measured with a vacuum gauge, was lowered to around 0.1 kP_a and the apparatus was allowed to sit for 20 hours in order to detect any leaks. Once leaks, if any, had been removed, then an adequate mass (25g) of distilled water was measured and introduced using a hypodermic syringe. For these experiments the charge was fixed as recommended by Chi [18]. The apparatus was then sealed and the experiments began.

Setting the heat pipe at the required position, the cooling water with fixed mass flow rate was turned on. Power to the heater was then set at a low level and the system was left to reach the steady state condition. This typically required a time period of about 1.5h, during which power adjustment were made, as necessary to establish reasonably steady wall temperatures. Once the system has stablilzed, readings were taken for temperatures of the vapor, wall, and the cooling water at both inlet and outlet. The gross power supplied, and the mass flow rate of cooling water were simultaneously recorded. It is worthnoting that, for each test run, an energy balance between the heat input by the heater and the heat removed by the calorimeter was monitored to ensure an energy balance of at least 90 percent during the steady-state operation. The power was then increased in discrete steps until temperature excursion occurred in the evaporation region and the above described procedure was repeated.

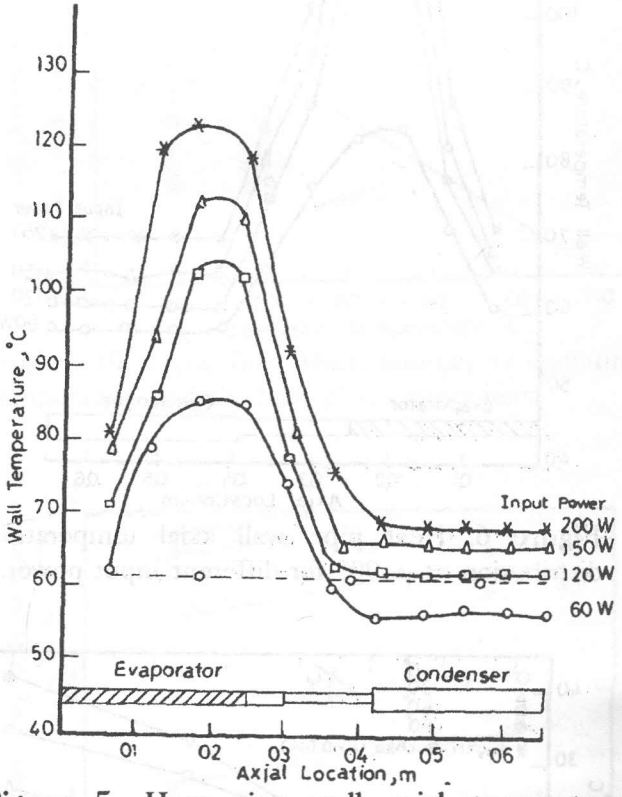

Figure 5. Heat pipe wall axial temperature-distribution at φ=0° for different input power.

RESULTS AND DISCUSSION

Figures (5) and (6) illustrate the experimental data of the wall temperature distributions along the heat pipe length for horizontal and vertical position respectively. It should be noted that, despite the

relative constant heat flux along the evaporator length, the peak wall temperature appears to be at the center of the active evaporator and decreases closer to the condenser. It should be noted, however that, the adiabatic section is unheated, it acts as an additional evaporator due to the axial heat conduction .

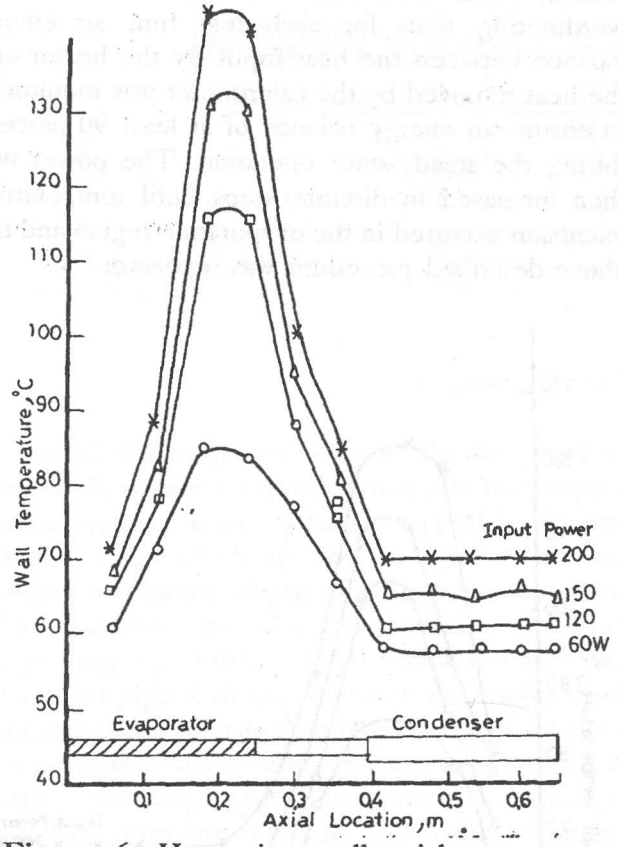

Figure 6. Heat pipe wall axial temperature distribution at φ=90° for different input power.

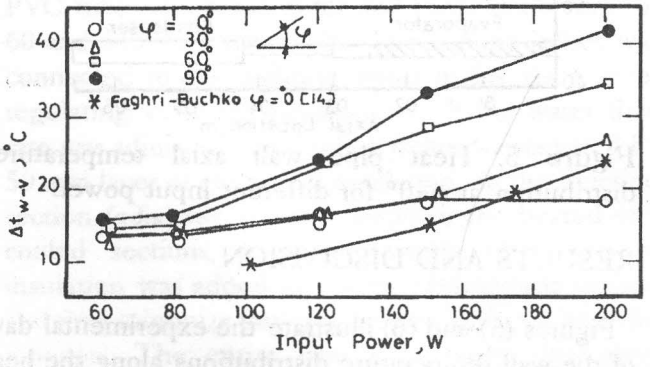

Figure 7. Wall-vapor temperature difference vs the input power for different heat pipe orientations.

Figure (7) shows the difference between the average evaporator wall temperature and the vapor temperature versus the input power. The plot of the tested data shows that Δt_{w-v} increases with both the input power and inclination angle at constant input power. The heat pipe in the vertical orientation (φ = 90°) exhibits the highest value of Δt_{w-v} when compared with other cases of less inclination angle.

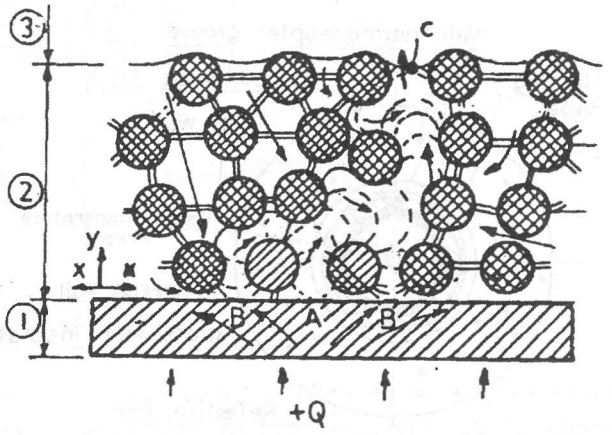

Figure 8. Approximate model of vaporization in screen matrix wicked heat pipe.
1- Heat pipe wall 2- Screen matrix 3- vapor core.

This phenomenon can be explained by understanding the mechanism of vaporization in a porous wick, Figure (8). The porous wick can be considered as a space of great number of meshes with various orientations. The mesh is simply depicted by four spherical particles connected by four heat ligaments which conductivity is considerably higher than that of liquid. The formation of a bubble occurs inside the mesh volume which serves as a center of nucleation. In the case of ($\varphi = 0^0$) (horizontal orientation) suppose that the formation of the bubble occurs at point (A). After its growth it separates from the surface at (A) through the open channel A-C (direction Y) to liquid-vapor interface. In this case, the liquid film at point (A) exposed to vaporization deserves small quantity of heat supplied from pipe wall and heat ligaments - or small temperature difference-to vaporize. It should also be noted that, due to the high conductivity of pipe wall and the wick, the unheated adiabatic section acts as an additional evaporating surface due to its wetted surface. On the contrary, in the case

of vertical position of the pipe, the bubble formed and grown at point (B) should be active untill the vapor film stops extending over the pipe wall in (X) direction. In the case of existence of low conductivity vapor film, the formation and growth of the bubble require some additional heat flux or greater temperature difference. Also, in such case (φ = 90°) the upper part of the evaporator suffers from surface dryness, hence the contribution of the unheated adiabatic section as additional evaporating surface should be ceased.

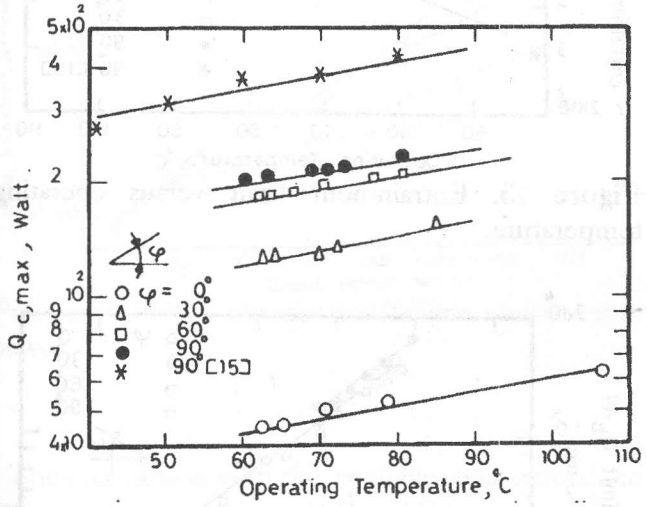

Figure 9. Maximum capillary heat transfer limit versus operating temperature.

Using Eq. 5, Figure (9) illustrates the predicted capillary heat transfer limit for the heat pipe with water as the working fluid, at different inclination angles. Similarly, for all heat pipe orientations, the results follow the same trend; the minimum transport capacity occurs at the minimum operating temperature. As shown in Figure (9), it is apparent that, on increasing the inclination angle, the heat pipe exhibits substantially increased capillary heat transport limit, which reaches its maximum value at vertical orientation $\varphi = 90°$. The enhancement in the heat transport capillary limit is due to increasing the maximum capillary pressure with greater inclination angles as a result of elevating the axial hydrostatic pressure. As it is mentioned before, the capillary limit calculated by Eq. 5, has been derived taking into account that, the vapor flow should be laminar and incompressible. For such conditions, the Mach number and vapor Reynolds number should not exceed 0.2 and 2300, respectively. In such conditions, the axial temperature gradient is negligibly small. Justification of the obtained data is shown in Figures (10 and 11). From these figures it is clear that, for all tested conditions, the heat pipe completely exhibits the condition of laminar and incompressible flow of vapor, described by Eqs.(7 and 8).

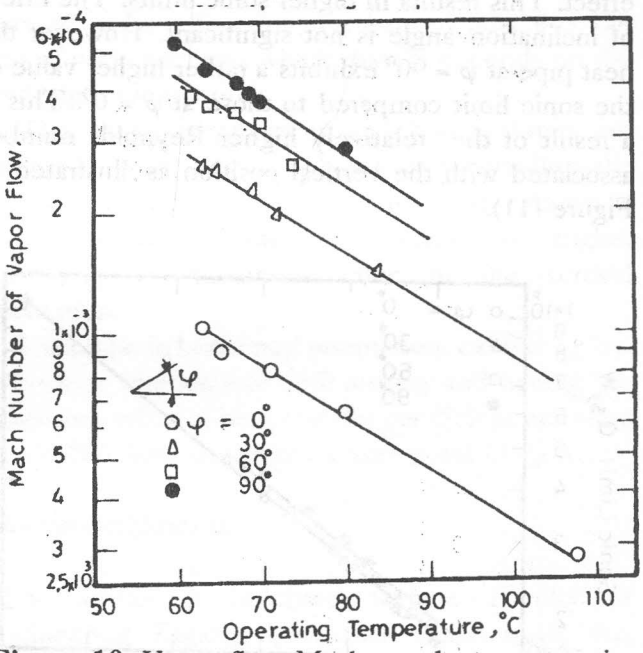

Figure 10. Vapor flow Mach number vs operating temperature and the heat pipe orientations.

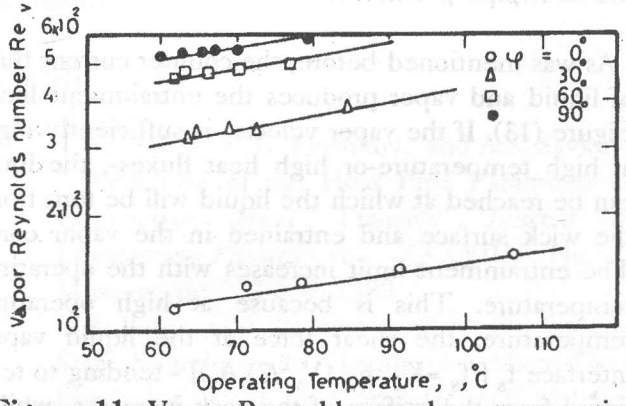

Figure 11. Vapor Reynolds number vs operating temperature and the heat pipe orientations.

Using Eq. (9), Figure (12) was prepared to illustrate, the predicted sonic heat transfer limit for the tested pipe for various inclination angles. As

seen, the results follow the same general trend, showing that the minimum sonic limit occurs at minimum operating temperature. This is because at lower temperature, the frictional effects are becoming more important and the sonic limit is considerably reduced. At higher temperatures, the high fluxes produce high Reynolds number of vapor at the evaporator yielding a rather small frictional effect. This results in higher sonic limits. The effect of inclination angle is not significant. However the heat pipe at $\varphi = 90^{o}$ exhibits a rather higher value of the sonic limit compared to those at $\varphi = 0^{o}$. This is a result of the relatively higher Reynolds number associated with the vertical position as illustrated in Figure (11).

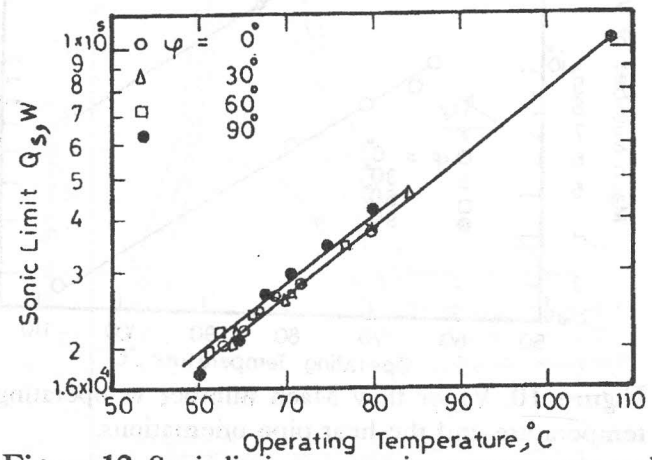

Figure 12. Sonic limit vs operating temperature and the heat pipe positions.

As was mentioned before, the counter current flow of liquid and vapor produces the entrainment limit Figure (13). If the vapor velocity is sufficiently high at high temperature-or high heat fluxes-, the limit can be reached at which the liquid will be torn from the wick surface and entrained in the vapor core. The entrainment limit increases with the operating temperature. This is because at high operating temperature, the shear force at the liquid vapor interface f_s [($f_s = K_1\ \rho_v . (V_v^2/2)\ A_s$)] - tending to tear liquid from the surface of the wick increases, whilst the surface forces f_t ($f_t = K_2\ \sigma\ C_s$) - which holds the liquid in the wick decreases. This was believed to be the reason for the increase in entrainment limit at high operating temperatures. The same picture -at a small scale- may be depicted at increased inclination angle. As it is also associated with increased vapor velocity or vapor Reynold number (Figure 11) together with an increase in the shear force f_s, the result is a small increase in entrainment limit.

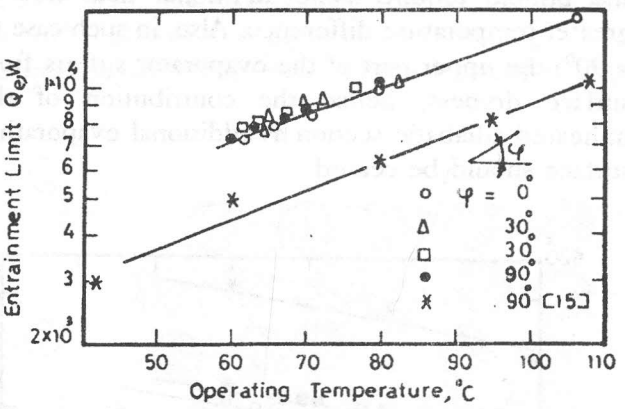

Figure 13. Entrainment limit versus operating temperature.

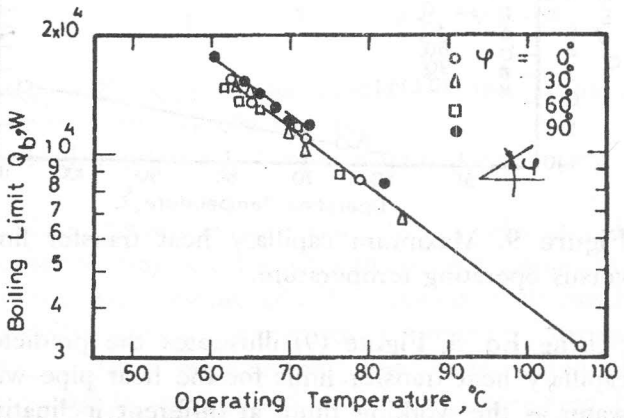

Figure 14. Boiling limit vs operating temperature.

Figure (14) illustrates the boiling limit versus operating temperature. As seen, the tested pipe is entirely in the boiling limit, and the maximum boiling capacity occurs at the minimum operating temperature. The degradation of the boiling limit along with formation of a small amount of noncondensible gas that occupies in the upper cap was considered the cause of the decrease in boiling limit at increased operating temperature. Also, it is assumed to be the result of nucleate bubble formation occuring in the evaporator wick. Once formed, these bubbles partially block a portion of the liquid return, thus reducing the effective area of the wick and hence decreasing the heat transport

boiling limit. As, it was observed before that there is very little change in the predicted boiling limit with changes in inclination angle. This finding coincides with that found by Babin and Peterson [4].

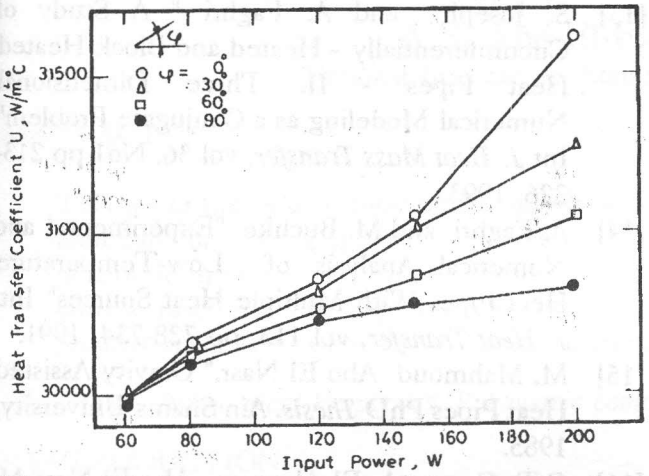

Figure 15. Heat transfer coefficient versus input power.

The comparison with the available results obtained by previous investigators [14] and [15] on water heat pipes in similar situations is shown in Figures (7,9 and 13). The differences between the present data and the previous works for similar conditions are believed to be due to the different experimental conditions namely pipe and wick structure.

When a heat pipe operates below its heat transfer limits its performance can be characterized by the coefficient of heat transfer Eq. (12). The predicted data are shown in Figure (15). As seen from the figure, at small input powers, significant difference on heat transfer coefficient values for various orientations are not significant. While tendency towards stronger differences is seen in the region of relatively high input powers. This is due to the excess in temperature differences revelent to the heat pipe at increased inclination angle as was mentioned before. Thus the highest values of heat transfer coefficient were found to belong to the heat pipe at horizontal orientation operating with minimum temperature difference.

CONCLUSIONS

A study on the thermal characteristics of a water copper heat pipe at various orientations was carried out. The summary of the results is given as follows.

- The mechanism describing the thermal characteristic of the heat pipe has been approximately stated.
- The evaporator wall-vapor temperature difference seemed to be a function not only of heat flux but also of wick wetness, which mainly depends on the heat pipe orientations.
- The sonic, entrainment and boiling limits are believed to be almost independent regarding the heat pipe orientation. The capillary limit is shown to be apparently affected by inclination angles, exhibiting its maximum value in the vertical orientation.
- Heat pipe in horizontal orientation, exhibiting low wall-vapor temperature differences, and having the maximum value of heat transfer coefficient are more acceptable from the heat transfer point of view.

Acknowledgments

The author is indebted to the Faculty of Engineering Zagazig University which made this work possible. The author also wishes to express his appreciation to professor, R.A Mahmoud and Professor K.A. EL Shorbagy, for their valuable comments.

REFERENCES

[1] V.F. Frolov, E.M. Pernikov, and A.S. Savkov, " Prediction of the Heat Pipe Parameter at Convective Heat Transfer" *Journal of Engineering-Physics* vol. XXXVIII, No 2, Moscow, pp 222-230, 1980.

[2] B.R. Babin, G.P. Peterson and D. Wu "Steady State Modeling and Testing of a Micro Heat Pipe". Int. *J. of Heat Transfer*, vol. 112 pp. 595-601, August 1990.

[3] G.P. Peterson, A.B. Duncan, M.A. Weichold, "Experimental Investigation of Micro Heat Pipes Fabricated in Silicon Wafers", Int. *J. of Heat Transfer*, vol. 115, pp. 751-765 - August

1993.

[4] B.R. Babin and G.P. Peterson "Experimental Investigation of a Flexible Bellows Heat Pipe for Cooling Discrete Heat Sources" Int. *J. of Heat Transfer*. vol. 112 pp 602-607 - 1992.

[5] B.J. Huang and J.T. Tsuei "A Method of Analysis for Heat Pipe Heat Exhangers "Int. *J. Heat Mass Transfer*. vol. 28 No 3 pp 553-562. 1985.

[6] Flavio Dobran "Suppression of the Sonic Heat Transfer limit in High-Temperature Heat Pipe" Int. *J. of Heat Transfer*, vol III. pp 605-610, 1989.

[7] K. Vafai and W. Wang "Analysis of Flow and Heat Transfer Characteristics of an Asymmetrical Flat Plate Heat Pipe" Int. *J. Heat Mass Transfer*, vol 35 No 9 pp 2087 - 2099. 1992.

[8] T. Yamamoto and Y. Tanaka "Experimental Study of Sodium Heat Pipes" Int. *J. JSME*, vol 30 No 269 pp 1776-1782. 1987.

[9] D.A. Pruzan, L.K. Kurgensmith, K.E Torrance and C.T. Avedisian "Design of High Performance Sintered-wick Heat Pipes" Int. *J. Heat Mass Transfer*, vol 34 No 6 pp 1417-1427, 1991.

[10] Yiding Coa and Amir Faghri "The Thermal Performance of Heat Pipes With Localized Heat Input" Int. *J. Heat Mass Transfer*, vol 32 No.7. pp 1279-1287, 1989.

[11] Ming-Ming Chen and Amir Farghri "An Analysis of Vapor Flow and the Heat Conduction Through the Liquid-Wick and Pipe Wall in a Heat Pipe With Single or Multiple Heat Sources" Int. *J. Heat Mass Transfer*, vol 33 No 9 pp 1845-1955, 1990.

[12] A. Farghri, M. Buchko and Y. Cao "A Study of High Temperature Heat Pipes With Multiple Heat Sources and Sinks: Part I. Experimental Methodology and Frozen Start-up Profiles" Int. *J. Heat Mass Transfer*, vol 113 pp. 1003 - 1009, 1991 .

[13] S. Joseph and A. Faghri " A Study of Circumferentially - Heated and Block-Heated Heat Pipes - II. Three Dimensional Numerical Modeling as a Conjugate Problem" Int *J. Heat Mass Transfer*, vol 36. No1 pp 213-226, 1993.

[14] A. Faghri and M. Buchko "Experimental and Numerical Analysis of Low-Temperature Heat Pipes With Multiple Heat Sources" Int. *J. Heat Transfer*, vol 113, pp 728-734, 1991.

[15] M. Mahmoud Abo El Nasr," Gravity Assisted Heat Pipes PhD *Thesis*. Ain Shams University, 1985.

[16] C.T. Crowe, A. El Ahwany, Abo El-Nasr M. and R. Abdel Aziz "Performance Limits of a Porous Heat Pipes", *Proceeding of Eighth International Conference For Mechanical Power Engineering Alexandria*, pp 253-261, 1993.

[17] S. Mohamed, El Genk, and Lianmin Huang "An Experimental Investigation of the Transient Response of a Water Heat Pipe" Int. *J. Heat Mass Transfer*, vol 36, No 16 pp 3823-3830, 1993.

[18] S.W. Chi. *Heat Pipe Theory and Practice*, A Sourcebook" McGraw-Hill, 1976.

[19] P.D. Dunn, and D.A. Reay, *Heat Pipe*. A source book In Russian Pergamon Press 1976.

[20] M.N. Ivanovski, V.P. Sorokin and I.V. Yagodkin, *Physical Principles of Heat Pipes*. A source book In Russian, Atom Press 1978.t